Sensors and Actuators B 140 (2009) 287–294

Contents lists available at ScienceDirect

Sensors and Actuators B: Chemical

journal homepage: www.elsevier.com/locate/snb

Electrokinetic actuation of low conductivity dielectric liquids

R.V. Raghavan [a], J. Qin [a], L.Y. Yeo [a,*], J.R. Friend [a], K. Takemura [b], S. Yokota [c], K. Edamura [d]

[a] Micro/Nanophysics Research Laboratory, Monash University, Clayton, Victoria 3800, Australia
[b] Department of Mechanical Engineering, Keio University, Yokohama, Japan
[c] Precision and Intelligence Laboratory, Tokyo Institute of Technology, Japan
[d] New Technology Management Co. Ltd., Tokyo, Japan

ARTICLE INFO

Article history:
Received 26 August 2008
Received in revised form 10 February 2009
Accepted 20 April 2009
Available online 3 May 2009

Keywords:
Microfluidics
Electrohydrodynamics
Micropumping
Electric pressure gradient
Induced charge
Polarization

ABSTRACT

Whilst electrohydrodynamic (EHD) flow actuation of dielectric fluids has been widely demonstrated, the fundamental mechanisms responsible for their behaviour is not well understood. By highlighting key distinguishing features of the various EHD mechanisms discussed in the literature, and proposing a more general mechanism based on Maxwell (electric) pressure gradients that arise due to induced polarization, we suggest that it is possible to identify the dominant EHD mechanisms that are responsible for an observed flow. We demonstrate this for a class of low conductivity dielectric fluids — Electro-Conjugate Fluids (ECFs) — that have recently been shown to exhibit EHD flow phenomena when subjected to non-uniform fields of low intensities. Careful inspection of the salient attributes of the flow, at least at low field strengths (<1 kV/cm) — for example, the absence of a threshold voltage for the onset of flow, the quadratic scaling of the flow velocity with the applied voltage, and flow from the high to the low field region — eliminate the possibility of mechanisms based on space charge. Instead, we suggest that flow can be attributed to the existence of a Maxwell pressure gradient. This is further corroborated by good agreement between our experimental results and theoretical analysis.

1. Introduction

The drive towards miniaturization of chemical and biological analytical systems has created the need for microfluidic actuation mechanisms such as micro-scale pumps, valves, reactors and separators [1]. Whilst a variety of fluid actuation schemes have been proposed, the absence of mechanical parts, lightweight construction, reliability, low power consumption and the ability to generate considerable flow velocities have led to electrohydrodynamics (EHD) as an obvious choice for actuation in heat transfer and micropumping devices involving dielectric fluids [2].

EHD flow is induced when a dielectric fluid is subjected to a non-uniform electric field. To date, several mechanisms have been proposed in order to explain the observed EHD phenomena, namely, ion injection, conduction pumping and induction pumping. Whilst the first two mechanisms rely on the presence of space charge in the fluid, the latter requires charge polarization to be induced within the fluid. It seems though that these mechanisms have been proposed almost in isolation to each other, perhaps as a result of their proponents working in widely different research disciplines. Moreover, few attempts have been made to discuss the differences between these mechanisms and to suggest specific circumstances under which a mechanism dominates over others. Consequently, this has resulted in considerable confusion in the literature.

In this paper we briefly discuss the underlying principles responsible for each of the mechanisms and summarize the key features that distinguish each of them. We believe that this will allow identification of the dominant mechanism underlying a specific EHD phenomenon. We do not *a priori* assume any of the mechanisms discussed above to be the dominant mechanism in our experiments. Instead, we allow our experimental observations and a theoretical analysis to determine this through a process of elimination. By doing so, we hope to demonstrate that it is possible to identify a dominant mechanism by comparing the salient features of the EHD flow with the key distinguishing attributes of the various EHD mechanisms that we will summarize in the conclusions of the paper. In addition, we also propose a more general mechanism that can generate EHD flows driven by Maxwell (electric) pressure gradients. We show that this is the dominant mechanism, at least when low electric field intensities are employed for a particular class of dielectric fluids known as Electro-Conjugate Fluids (ECF) that have recently been used in several EHD applications [3–5]. Our motivation behind the choice of these fluids was the lack of fundamental understanding regarding their mode of actuation. From a generic viewpoint, these fluids may be treated as typical low conductivity homogenous dielectric liquids.

* Corresponding author. Tel.: +61 3 99053834; fax: +61 3 99054943.
E-mail address: leslie.yeo@eng.monash.edu.au (L.Y. Yeo).

0925-4005/$ – see front matter © 2009 Elsevier B.V. All rights reserved.
doi:10.1016/j.snb.2009.04.036

The rest of this paper is organized as follows. In Section 2, we briefly discuss the three EHD mechanisms that have been reported, albeit almost independently, in the literature. The possibility of driving EHD flow through Maxwell pressure gradients is then discussed in Section 3, where we also develop the underlying theory associated with it. Details of the experimental procedure used to investigate the EHD flow of ECFs is described in Section 4. Subsequently, we report on the experimental observations in Section 5 and proceed to discuss the relevant dominant mechanisms that pertain to our particular experiments. Finally, we summarize the key attributes of the various EHD mechanisms in Section 6.

2. Electrohydrodynamic actuation mechanisms

The electric body force density acting on a liquid is described by the Korteweg–Helmholtz equation [6]:

$$\mathbf{F_e} = q_v\mathbf{E} - \frac{1}{2}\nabla\left[\epsilon - \frac{1}{2}\nabla\rho\left(\frac{\partial\epsilon}{\partial\rho}\right)_T\right]\mathbf{E}\cdot\mathbf{E}, \quad (1)$$

where q_v, ϵ, ρ, $\mathbf{E}$ and T refer to the net volume charge density, fluid permittivity, fluid density, applied electric field and a condition of constant temperature, respectively. The first term in Eq. (1) accounts for the Coulombic force exerted on free charges in the liquid in the presence of an electric field. The second term refers to a dielectric force which is induced in the presence of a permittivity gradient. For example, the presence of a liquid/vapour or liquid/liquid interface or the existence of non-isothermal conditions or electric inhomogeneity in a single phase liquid can generate the required permittivity gradient. The third term arises due to electrostriction effects which occur in compressible media. Hence, in the absence of an external pressure gradient, a weakly conducting, incompressible dielectric fluid in the presence of an electric field can be forced to flow only if space charges are generated in the fluid or if there exists a permittivity gradient across the field. These two principles therefore form the basis of all the EHD actuation mechanisms to be discussed.

2.1. Ion injection

As its name suggests, the ion injection mechanism involves the direct injection of charges into an insulating dielectric fluid through a corona source, as shown in Fig. 1 [7]. The injected unipolar charges are forced to migrate away from the corona source by the electric field and, in the process, drag molecules of the bulk fluid along, giving rise to a net flow. Hence, ion injection is also commonly referred to as *ion drag pumping*. This was first proposed by Stuetzer [8] in the late 1950s and has since been implemented in numerous micro-cooling and micropumping devices [9,10]. Ion injection is commonly used in situations that demand high pressure heads where the degradation of the working fluid is of little importance. A disadvantage, however, is the large field strengths commensurate with the threshold ionisation voltages, typically 100 kV/cm, required to drive the mechanism [11].

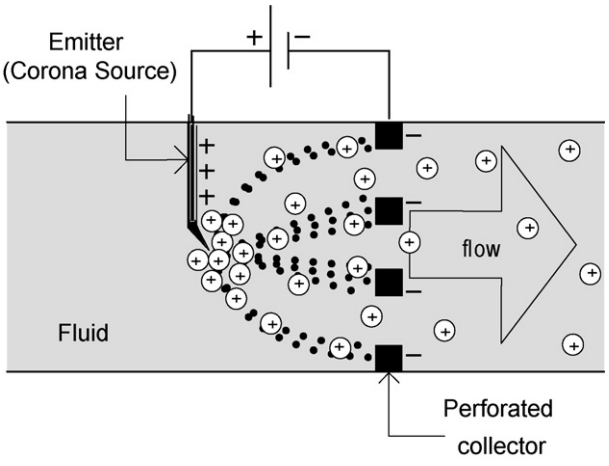

Fig. 1. Schematic illustration of the ion injection pumping mechanism.

A typical ion drag pump utilises a sharp needle-like corona source, a perforated or hollow collector electrode and an insulating working fluid to maximise efficiency [13]. The injected charges experience a Coulombic force as a result of the electric field created by the electrode arrangement. Consequently, the motion of these charges away from the high field region induces bulk flow in the insulating fluid in the same direction. Fig. 1 illustrates a generic ion drag pump configuration.

The drift velocity $\mathbf{v}$ of an ion in an electric field is given by

$$\mathbf{v} = b\mathbf{E}, \quad (2)$$

where b refers to the ion mobility in the fluid. Taking bulk flow into account allows us to rewrite Eq. (2) as

$$\mathbf{v} = b\mathbf{E} + \mathbf{u}, \quad (3)$$

where $\mathbf{u}$ refers to the fluid velocity. Hence, the expression for the current density, $\mathbf{j}$, in an ion drag pump becomes

$$\mathbf{j} = (b\mathbf{E} + \mathbf{u})q_v, \quad (4)$$

where q_v is the net volume charge density. Neglecting inertial and viscous forces, the pressure gradient along the longitudinal axis x, which gives rise to EHD flow as a consequence of the Coulombic force arising due to the longitudinal component of the electric field E_x is

$$\frac{\partial p}{\partial x} = q_v E_x. \quad (5)$$

Using Eq. (4) and noting that $j = I/A$ where I is the current and A the cross-sectional area, we can eliminate q_v from Eq. (5) to obtain

$$\frac{\partial p}{\partial x} = \frac{I_x}{Ab}. \quad (6)$$

Integrating Eq. (6) across the length of the channel x to x_0 gives us Chattock's relation,

$$p - p_0 = \frac{I_x}{Ab}(x - x_0). \quad (7)$$

For the setup shown in Fig. 1, the electric field E and space charge q_v are related by the Poisson equation, i.e.,

$$\frac{\mathrm{d}E}{\mathrm{d}x} = q_v/\epsilon. \quad (8)$$

Together with Eqs. (5) and (6), it follows that $I_x/A = q_v b E_x$, which upon integrating over channel length x to x_0 to eliminate q_v, results in

$$E^2 - E_0^2 = \frac{2I_x}{Ab\epsilon}(x - x_0). \quad (9)$$

By comparing the above equation with Eq. (7) it can be shown that,

$$p - p_0 = \frac{\epsilon}{2}(E^2 - E_0^2), \quad (10)$$

where p_0 is the pressure at a reference position x_0. Eq. (10) thus suggests that the pressure scales with the square of the applied electric field and hence the applied voltage [8]. From Eq. (2), it is also evident that the fluid velocity generated by the migration of ions scales linearly to the applied voltage.

An ion drag pump can function in two modes: field ionisation and field emission. The former requires a setup similar to that shown in Fig. 1, i.e., with the high-voltage end connected to the emitter. In this case, the high field strength causes the electrons

to be drawn from the surrounding fluid to the emitter creating a collection of positively charged ions that are repelled away from it. Field emission occurs with electrons being injected into the liquid when the emitter is negatively polarized [14]. In both cases, ion drag pumping is characterised by bulk flow in the direction of the field, large currents and the existence of a threshold field strength below which flow will not occur [11,12].

2.2. Conduction pumping

In a manner similar to ion drag pumping, bulk flow due to conduction pumping also requires the presence of space charge in the fluid. However, the two rely on markedly different methods of charge generation. Onsager [15] showed that the increase in the ion dissociation rate of weak electrolytes (low conductivity dielectrics) in the presence of an electric field is proportional to the field strength and inversely proportional to the dielectric constant of the fluid. Reiss [16] further adapted this theory to attribute charge generation in dielectrics to the dissociation of trace polar impurities in the fluids and, in some cases, the molecules of the dielectric themselves. More recently, Seyed-Yagoobi et al. [2,11,17], conducted several theoretical and experimental studies on the effectiveness of this phenomenon for pumping fluids.

Conduction pumping of low conductivity dielectrics involves the formation of bipolar charges by the Faradaic dissociation of either polar impurities or the dielectric molecules, or a combination of both [18]. As in the case of ion drag pumping, the electromigration of these charges then induces bulk flow in the liquid. Fig. 2 shows how a pressure gradient is established due to the asymmetric migration of the cations and anions in a conduction pump. Counter-ions migrate towards the corresponding electrodes to create heterocharge layers with thicknesses proportional to the permittivity of the working fluid and the applied voltage [17].

Like the ion drag pump, the operation of a conduction pump is governed by equations similar to Eqs. (2)–(10). Consequently, the fluid velocity in a conduction pump also scales linearly with the applied voltage whilst the pressure scales with the quadratic of the voltage. Since bipolar conduction occurs in a conduction pump, net flow can arise only if the electrode configuration is asymmetric or if a non-uniform field is established within the fluid. Conduction pumping is characterised by fluid flow towards the high field region and by the existence of a field strength threshold that is typically 1 kV/cm, a value that corresponds to the minimum field strength required for the hydrogen bonds in the dielectric molecules to be broken and hence for the ionisation of the fluid to take place.

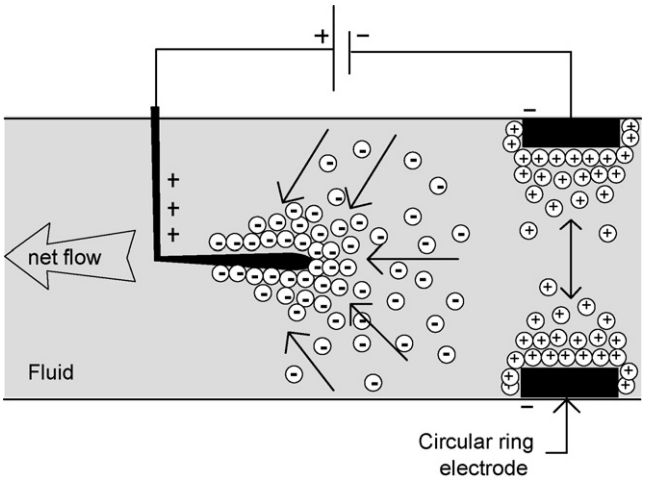

Fig. 2. Schematic illustration of the conduction pumping mechanism.

Regardless of whether it is the dissociation of impurities or the dielectric molecules, the formation of heterocharge layers would eventually reach Poisson–Boltzmann equilibrium, wherein the liquid around the electrodes would be shielded from the electric field by the charge layers in a manner similar to Debye layer screening in DC electrokinetics of conducting liquids. In a DC driven pump, this would prevent further ionisation, restricting the mechanism to operate only over short transients. However, if AC fields are employed, non-equilibrium field-induced charging effects will prevent the formation of heterocharge layers and permit pumping to continue [19].

2.3. Induction pumping

EHD induction pumps were first suggested by Melcher [20] as a means of actuating insulating fluids without having the electrodes physically in contact with them. This mechanism relies on the induction of surface charge in a dielectric owing to a conductivity or permittivity gradient across an interface. Although most induction pumps would require the presence of an interface between two media of different electrical properties, thermal gradients in a single phase fluid have also been exploited to create a discontinuity in conductivity [3,21].

The absence of charge injection in the process limits the amount of electric current and hence implies negligible interference from magnetic induction, permitting the assumption of an irrotational field [20]. As a result, the following interfacial boundary conditions, in which the tangential field is assumed to be continuous across the interface and the jump in the normal component of the electric displacement across the surface is given by the net surface charge q_s apply:

$$[E_t]_l^g = 0, \tag{11}$$

$$[\epsilon E_n]_l^g = q_s. \tag{12}$$

In the above, the subscripts n and t refer to the normal and tangential components of the electric field, respectively, and the square parentheses describe the jump in the inner quantities across an interface, evaluated by subtracting the inner quantity in the liquid phase (l) from that in the gas phase (g).

Conservation of momentum requires

$$\rho\left(\frac{\partial \mathbf{u}}{\partial t} + \mathbf{u}\cdot\nabla\mathbf{u}\right) = \nabla\cdot\mathbf{T}, \tag{13}$$

where $\mathbf{T}$ represents the total stress tensor such that

$$\nabla\cdot\mathbf{T} = -\nabla p + \nabla\cdot\mathbf{T_V} + \nabla\cdot\mathbf{T_M}. \tag{14}$$

Here $\mathbf{T_V}$ is the viscous stress and ∇p accounts for the pressure gradient due to external sources. The expression for the viscous stress tensor is

$$\nabla\cdot\mathbf{T_V} = \mu[\nabla\mathbf{u} + \nabla\mathbf{u}^T], \tag{15}$$

in which μ refers to the fluid viscosity and $\nabla\mathbf{u}^T$ refers to the transpose of the velocity gradient vector.

$\mathbf{T_M}$, on the other hand, is the Maxwell stress tensor, which can be derived from the definition of the electric displacement $\mathbf{D}$ for a linear dielectric,

$$\mathbf{D} = \epsilon_o(1+\chi_e)\mathbf{E} = \epsilon_o\epsilon_r\mathbf{E} = \epsilon\mathbf{E}, \tag{16}$$

where ϵ_o is the permittivity of free space, χ_e is the electrical susceptibility and ϵ_r is the relative permittivity of the fluid, together with Gauss' Law $\nabla\cdot(\epsilon\nabla\varphi) = -q_v$ in which φ is the electric potential. When inserted into the Korteweg–Helmholtz equation given by Eq.

(1), this becomes

$$\mathbf{F_e} = (\nabla \cdot \mathbf{D})\mathbf{E} - \frac{1}{2}\mathbf{E} \cdot \mathbf{E}\nabla\epsilon, \tag{17}$$

for an incompressible medium. With some vector manipulation, it then follows that

$$\mathbf{F_e} = (\nabla \cdot \mathbf{D}\mathrm{E}) - \tfrac{1}{2}\nabla(\epsilon\mathbf{E} \cdot \mathbf{E}) + \epsilon\mathbf{E} \cdot \nabla\mathbf{E}, \tag{18}$$

which from Eq. (16), can be expressed as

$$\mathbf{F_e} = \nabla \cdot (\epsilon\mathbf{E}\mathrm{E} - \tfrac{1}{2}\epsilon(\mathbf{E} \cdot \mathbf{E})\mathbf{I}), \tag{19}$$

where $\mathbf{I}$ is the second-order identity tensor. Eq. (19) can be expressed in terms of a divergence of the Maxwell stress tensor

$$\mathbf{F_e} = \nabla \cdot \mathbf{T_M}, \tag{20}$$

and hence a comparison between Eqs. (19) and (20) gives an expression for the Maxwell stress tensor [22,23], which reads

$$\mathbf{T_M} = \epsilon\mathbf{E}\mathrm{E} - \tfrac{1}{2}\epsilon(\mathbf{E} \cdot \mathbf{E})\mathbf{I}. \tag{21}$$

The jump in the normal and tangential components of this tensor across the interface is then

$$\mathbf{T_{M_n}} = \mathbf{n} \cdot \mathbf{T_M} \cdot \mathbf{n} = \tfrac{1}{2}[\epsilon E_n^2 - \epsilon E_t^2]_l^g, \tag{22}$$

$$\mathbf{T_{M_t}} = \mathbf{n} \cdot \mathbf{T_M} \cdot \mathbf{t} = [\epsilon E_n]_l^g E_t = q_s E_t, \tag{23}$$

where $\mathbf{n}$ and $\mathbf{t}$ are the unit normal and tangential vectors. The resulting electric stress is evaluated by calculating the difference between the inner quantities in the gas and liquid phases.

From Eq. (23), it can be seen that the interaction between the induced charge and the tangential field at the interface gives rise to an interfacial tangential shear that drags the fluid along. Balancing the viscous drag at the interface with this tangential shear force and the no-slip condition at the contact surface allows the derivation of an expression for steady state velocity which reveals a quadratic dependence on the applied voltage [20,21].

Fig. 3 provides a graphical representation of induction pumping in action. The slanted electrode provides the required normal field (dashed lines) through the interface that in turn induces interfacial charges of opposite polarity. The tangential field generated within the body of fluid exerts a force upon this charge layer resulting in interfacial stresses and hence, flow is established in the direction of the field. In the setup shown in the figure, fluid recirculation is observed since flow is established in a closed channel.

It can be seen from Eq. (23) that the length scale over which the fluid is driven is commensurate with that across which the interfacial charge and tangential field is spatially distributed. A highly conductive fluid in which charge relaxation is almost instantaneous does not support induction pumping. Similarly, if the conductivity is too small, few charges relax to the surface and the shear generated is negligible [20]. Hence, an important point to note is that induction pumping is not suitable for low conductivity dielectrics ($\ll 10^{-8}$ S/m) as they do not support adequate surface charge generation.

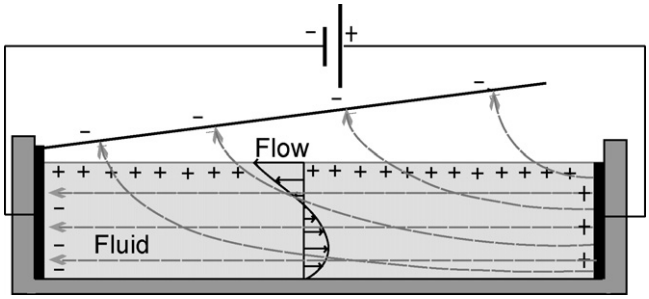

Fig. 3. Schematic illustration of the induction pumping mechanism.

3. Fluid flow driven by Maxwell pressure gradients

EHD flow can also be induced if an electric pressure gradient is established within a liquid through the application of a non-uniform electric field. In fact, induction pumping, explained in the previous section is a special case of this mechanism which utilizes a gradient in the tangential Maxwell stress $\mathbf{T_{M_t}}$. Generalisation of the induction pumping mechanism to the broader Maxwell pressure gradient driven flow mechanism then accounts for similar EHD flow behaviour in the absence of interfacial charge. In situations where low conductivity leads to negligible surface charge at the interface, Eq. (12) then becomes

$$[\epsilon E_n]_l^g \approx 0. \tag{24}$$

As a result, the tangential component of the Maxwell stress tensor in Eq. (23) then becomes negligible. Maxwell pressure gradient driven bulk flow may arise even in the absence of interfacial charge owing to the gradient in the normal component of the Maxwell stress tensor given in Eq. (22). Depending on the setup of the pump, either the tangential or the normal field, and, in some cases a combination of both may be responsible for the Maxwell stress $\mathbf{T_M}$ that appears in Eq. (14). It is important to note that this mechanism does not necessarily have to arise through interfacial stresses.

This can be better understood through Fig. 4, wherein the non-uniform electric field (dashed lines) produced by the pin-plate electrode configuration gives rise to a Maxwell pressure gradient which drives the flow. For microchannel flows, the vertical length represented by the liquid height h is usually much smaller than the channel length L. For these small aspect ratios ($\delta \equiv h/L \ll 1$), the gradient in the electric field in the normal direction is usually much larger than that in the tangential direction, and, as such, the latter can be neglected. For incompressible fluid flowing through a channel of rectangular geometry (Fig. 4), it then follows (assuming that the effects of curvature at the free surface are negligible) that Eq. (13) together with Eqs. (14) and (21) reduce to

$$\mu\frac{\partial^2 u}{\partial y^2} = \frac{\epsilon}{2}\frac{\partial {E_n}^2}{\partial x} + \frac{\partial p}{\partial x}. \tag{25}$$

Cho et al. [24] describe the electric field generated by a pin-plate arrangement using a polar coordinate system, where r refers to the distance between the emitter tip and a point on the plane electrode, V is the applied voltage and θ is the angle subtended by the radius from the vertical. The radial component of this electric field is given by

$$E_r = V\left[\frac{1}{r} + \frac{(2d\cos\theta - r) + \sqrt{a}}{a + (2d - r\cos\theta)\sqrt{a}}\right], \tag{26}$$

where

$$a = 4d^2 - 4dr\cos\theta + r^2. \tag{27}$$

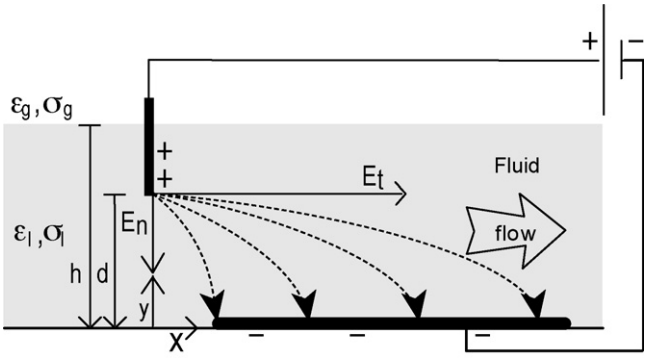

Fig. 4. Schematic to illustrate how Maxwell pressure gradient driven flow may arise.

In Eqs. (26) and (27), d is the vertical distance between the emitter and the plate. When $\theta = 0$ ($r = d$), Eq. (26) provides an expression for the axial field created by the pin-plate such that

$$E_r = V\left[\frac{1}{r} + \frac{1}{2d - r}\right] = \frac{2V}{r}. \tag{28}$$

For the experimental setup shown in Fig. 4, Eq. (28) can be rewritten as

$$E_n = \frac{2V}{\sqrt{x^2 + d^2}} \approx \frac{2V}{x}, \quad \text{since } d \ll x. \tag{29}$$

To render the problem dimensionless, we employ the following transformations: $u \to \bar{u}U_0$, $V \to \bar{V}V_0$, $x \to \bar{x}L$, $y \to \bar{y}h$, where $U_0 = 2\epsilon V_0^2\delta^2/\mu L$ is the characteristic velocity obtained through an electroviscous scaling that balances the dominant viscous and Maxwell (electric) forces. Here, V_0, h and L are the characteristic voltage, height and length parameters that are given values based on our experimental setup. In our derivations, overbars have been used to denote dimensionless quantities. In the absence of an externally imposed pressure gradient $\partial p/\partial x$, Eq. (25), in dimensionless form may be written as

$$\mu\frac{U_0}{\delta^2}\frac{\partial^2\bar{u}}{\partial\bar{y}^2} = \frac{\epsilon V_0^2}{2L}\frac{\partial}{\partial\bar{x}}\left(\frac{4\bar{V}^2}{\bar{x}^2}\right). \tag{30}$$

We now integrate Eq. (30) with the following no-slip and shear free boundary conditions at the substrate and free surface, respectively:

$$\bar{u} = 0 \quad \text{at } \bar{y} = 0, \tag{31}$$

and

$$\frac{\partial\bar{u}}{\partial\bar{y}} = 0 \quad \text{at } \bar{y} = \bar{h}. \tag{32}$$

This results in the relation

$$\bar{u} = \frac{2\epsilon V_0^2\bar{V}^2\delta^2}{\mu\bar{x}^3 L U_0}(2\bar{h}\bar{y} - \bar{y}^2). \tag{33}$$

Further, substituting for U_0 in the expression above results in

$$\bar{u} = \frac{\bar{V}^2}{\bar{x}^3}(2\bar{h}\bar{y} - \bar{y}^2). \tag{34}$$

Owing to flow continuity, integrating the above expression over the channel height $\bar{h}$ and length $\bar{L}$ results in the average velocity such that

$$\langle\bar{u}\rangle = \tfrac{1}{3}\bar{V}^2. \tag{35}$$

Eq. (35) indicates a quadratic dependence between the fluid velocity and the applied voltage. The characteristic height h, length L and voltage V_0 of the system have been chosen to be 0.003 m, 0.03 m and 1 kV. These values have been chosen as they correspond to the parameters used in our experiments which were set up in a manner similar to that shown in Fig. 4. The redimensionalisation of Eq. (35) results in

$$\langle u\rangle = \frac{2\epsilon\delta^2}{3\mu L}V^2, \tag{36}$$

which describes how the average fluid velocity in the channel depends upon the intrinsic properties of the working fluid.

4. Experimental setup

Fig. 5 shows an isometric and lateral view of the experimental setup. The channels were machined into a circular piece of transparent acrylic so that the motion of the fluid could be observed from underneath using an inverted microscope. A 5 mm square channel was cast through the central part of the device in a manner that allowed recirculation of fluid as it was pumped. The bottom surface

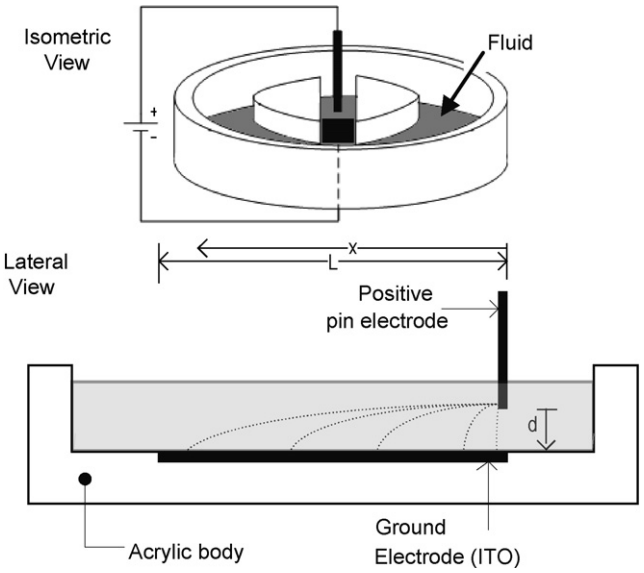

Fig. 5. Illustration of the experimental setup.

of the channel was constructed out of glass coated with indium tin oxide (ITO) to permit visualisation and also to function as the conducting ground electrode. A titanium pin was mounted at the opening of the channel such that its tip was at a height d above the surface of the plane electrode. The pin acts as an emitter, setting up a non-uniform electric field across the entire channel length L when connected to a voltage source.

Unlike electroosmotic pumps where electrodes are placed at both ends of the fluidic channel, the positively charged pin electrode in Maxwell pressure gradient-driven pumps must be placed at the opening of the channel in order to establish the required Maxwell pressure gradient. If the pin is placed in the middle of the channel, no net flow will result, as pressure gradients are generated towards both ends of the channel resulting in bidirectional flow away from the centre. In order to prevent the occurrence of ion injection, the pin was coated with Teflon® AF (601S1-100-6, DuPont, USA) and its tip was ground smooth. The tip of the electrode was positioned well below the liquid-gas interphase whilst also maintaining a gap $d = 1$ mm to the surface of the ground electrode. This ensured that the field was predominantly in the liquid phase in order to minimize the electric displacement across the interface. Hence, as stipulated by Eq. (24), the interfacial charge at the free surface is negligible since the field is mainly tangential at the interface.

The theoretical predictions in Eqs. (35) and (36) were verified through high speed video microscopy using an inverted fluorescence microscope (IX71, Olympus, Tokyo, Japan) connected to a high speed camera (Hisense MKII, Dantec Dynamics, Skovlunde, Denmark) capable of imaging at 32000 frames/s. To aid visualization, the flow field was seeded with 8 μm particles (36-3 fluorescent polystyrene particles, Duke Scientific, California, USA) which were illuminated with a Nd:Yag laser unit (New Wave Research, CA, USA) operating at 532 nm. In order to calculate the flow velocities of the fluid for different applied voltages (0–5000 V), the high speed camera was used to capture the motion of the particles within the flow field in two successive images separated by a known time frame. These images were then used to evaluate the particle trajectories and velocities using FlowMap®, a particle tracking software (Dantec Dynamics, Skovlunde, Denmark). In each of these measurements, the focal plane was positioned at the midplane height of the fluid in the channel as shown in Fig. 6.

As alluded to in Section 1, the DC electric-field pumping of a class of low conductivity dielectric fluids, termed as electro-conjugate

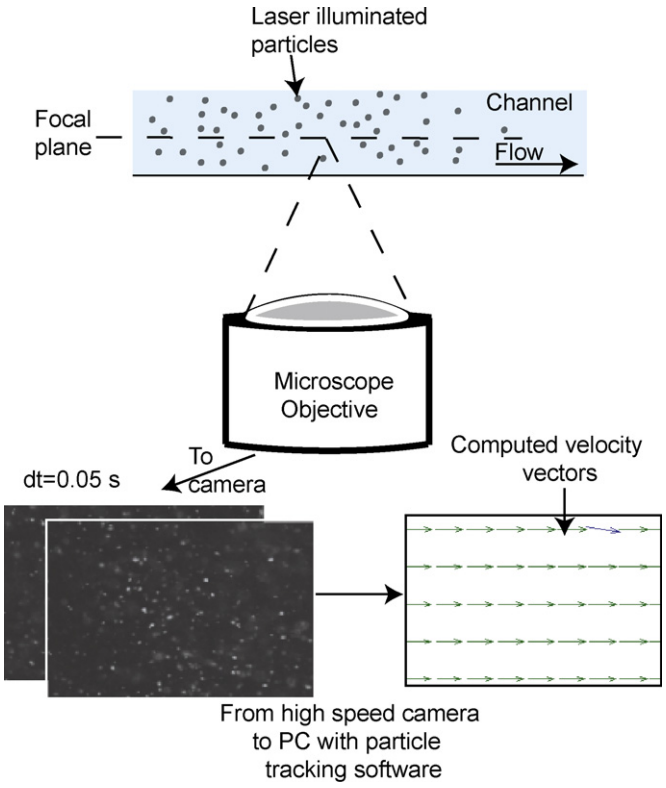

Fig. 6. Microparticle image velocimetry setup used to calculate the flow velocities.

fluids (ECFs) [5,6] has recently been demonstrated. Since the mechanism by which these fluids were actuated was not understood, we chose the actuation of these fluids as a test case to identify the dominant EHD mechanism responsible for flow, by comparing experimental results with the known attributes of the various EHD mechanisms discussed. Three fluids that conformed to the characteristics of ECFs were thus chosen as the working fluids for our experiments. The fluid properties of the specific dielectrics used in this study are detailed in Table 1 [26]. Both the working fluid and the fluorescent particles were replaced after each experiment to avoid contamination and agglomeration of the particles.

Since dielectric particles within a dielectric medium experience dielectrophoresis (DEP) [25], the particle DEP velocities u_{DEP} have to be accounted for when determining the true flow velocity u from the apparent (observed) particle velocity u_{app}. Employing an expression for the electric field strength given by that in Eq. (29), the DEP particle velocity is given by

$$u_{DEP} = \frac{4\epsilon_l a^2 \mathrm{Re}[f_{cm}]V^2}{3\mu x^3}, \tag{37}$$

where a refers to the particle diameter and x the distance along the channel to the position where the velocity measurements were made which, in our case is 0.01 m. The conductivities of the fluid σ_l, and of the particles σ_p, are used to calculate the Clausius–Mosotti factor f_{cm}, which determines the direction of the DEP force, i.e., positive or negative:

$$\mathrm{Re}[f_{cm}] = \mathrm{Re}\left[\frac{\sigma_p - \sigma_l}{\sigma_p + 2\sigma_l}\right]. \tag{38}$$

Only the real part of the Clausius–Mossotti factor is relevant to our calculations since we employ DC fields in our experiments. For the particles and the media used, the electrical properties for which have been obtained from [26–28], the calculation yields a negative value indicating that the particles tend to move towards the region of lower field strength, i.e., in the direction of the Maxwell pressure gradient-driven flow. Hence,

$$u = u_{app} - u_{DEP}. \tag{39}$$

Although u_{DEP} values have been taken into account, we note that they are much smaller than the fluid velocities and typically on the order 10^{-7} to 10^{-5} m/s, and thus the DEP contribution to the particle motion can be neglected.

Table 1
Properties of the dielectric fluids used in the experiments.

Name	Conductivity ($\times 10^{-10}$ S/m)	Viscosity ($\times 10^{-3}$ Pa s)	Permittivity ($\times 10^{-11}$ F/m)
Dibutyl decanedioate	4.7	7.0	4.54
Linalyl acetate	18.2	1.3	4.46
Dibutyl adipate	30.1	3.5	4.6

5. Results and discussion

In Fig. 7, the dashed lines represent the theoretical predictions for each fluid using Eq. (36) whilst the markers represent the experimental data obtained. The experiments revealed the generation of unidirectional flow *away* from the high field region. In addition, we observe a linear relationship between fluid velocity and the square of the applied voltage, as shown in Fig. 7. Moreover, we also note the absence of a critical threshold voltage for the flow to commence; a flow appears at any non-zero voltage.

The non-linear relationship between the fluid velocity and voltage suggests that the ion injection and conduction pumping mechanisms are not major contributors to flow, at least for the conditions simulated in our experiments. Furthermore, fluid flow due to ion injection and conduction pumping only commences beyond threshold electric field intensities of 100 and 1 kV/cm, respectively. Neither of these thresholds were reached in our experiments and yet we still observed fluid flow.

The absence of a threshold voltage for flow and the quadratic velocity scaling with respect to the applied voltage, however, does not exclude induction pumping a possible mechanism. It must be noted that induction pumping would require the generation of spatial charge distribution at the interface, for which, the established normal field would have to cut across the interface. However, the experimental setup employed minimizes the electric flux across the interface hence allowing us to neglect the possibility of interfacial charging. Furthermore, we found that flow persisted despite the absence of a free surface, thus allowing us to eliminate induc-

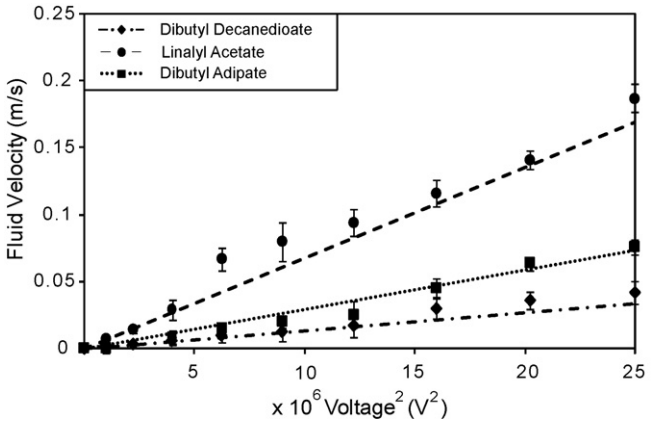

Fig. 7. Theoretical and experimental fluid velocity as a function of the square of the applied voltage.

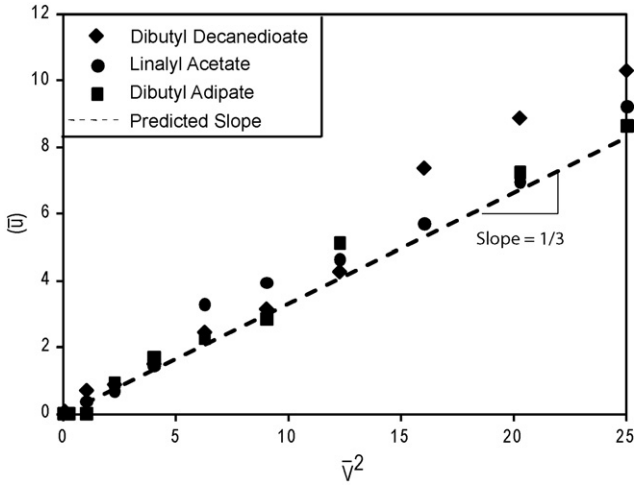

Fig. 8. Collapse of the experimental data using the electroviscous velocity scaling in Eq. (35) as a function of the dimensionless voltage squared.

tion pumping as the driving mechanism. These observations then provide clear evidence that suggest that the Maxwell pressure gradient mechanism is responsible for the generation of flow in our experiments.

The evidence of the flow being driven by Maxwell pressure gradients is further strengthened by good agreement between the experimental results and the theoretical prediction given by Eq. (36). Accordingly, the slopes obtained are observed to be proportional to the ratio of the fluid's permittivity to its viscosity.

Fig. 8 depicts a collapse of the experimental fluid velocity data using the electroviscous scaling model. The slope predicted in Eq. (35) corroborates well with the experimental data (markers) shown in the figure, verifying the obvious balance between the electric and viscous force as expected in EHD flow driven by the Maxwell pressure gradient mechanism. This not only adds further credence to the Maxwell pressure gradient mechanism, but also validates the model.

An important point to note is that, it is possible for one particular EHD flow mechanism to dominate flow generation under certain conditions, and for another to come into effect under slightly different conditions, even if the same fluid and experimental setup are employed. For example, with our setup, it is quite possible that ion injection becomes the principle mechanism that drives flow at higher electric field intensities when the threshold ionization voltage is exceeded, resulting in the generation of space charge.

6. Conclusion

Through experiments and theoretical analysis, we have sought to elucidate a fundamental understanding of the mechanism that is responsible for the electrohydrodynamic flow actuation of a particular class of homogenous dielectric fluids that have been termed as Electro-Conjugate Fluids (ECFs) [3–5]. The absence of a critical threshold voltage for the commencement of flow, the quadratic scaling of the flow velocity with respect to the applied voltage and the flow direction allowed us to eliminate existing EHD mechanisms in the literature, namely, ion injection and conduction pumping which require the introduction of space charge into the fluid by some means or the other and hence impose threshold voltages that need to be exceeded for flow to commence. Moreover, the linear relationship between the voltage and velocity in these mechanisms is inconsistent with the experimental results obtained. In addition, the flow direction observed, which is from the high to the low field region, is opposite to that in conduction pumping.

Table 2
Attributes of the various EHD pumping mechanisms.

Mechanism	Threshold (kV/m)	$\mathbf{u} \propto$	Flow direction
Ion injection	10^4	V	High field to low
Conduction	10^2	V	Low field to high
Induction	0	V^2	Either direction
Maxwell pressure gradient	0	V^2	High field to low

The ability to drive flow in the absence if a free surface and interfacial charge also suggests that a more general dielectric polarization mechanism than that associated with induction pumping is at play. In fact, the results we observe consistently point towards the role of Maxwell pressure gradients in driving the EHD flow, at least at the low field intensities employed. Furthermore, good agreement is obtained between the experimental results and the analytical model developed.

Whilst we have carried out experiments for a particular class of dielectric fluids, we postulate that the results obtained apply for more general low conductivity dielectric fluids as well. The theory developed and verified, suggests that the flow behaviour is dominated by the permittivity and viscosity of the fluid. Regardless of the fluid's properties, the salient features of the EHD flow, i.e., the absence of a threshold voltage, the quadratic dependence of the velocity on the voltage and the flow direction from high to low field intensity regions, remain unchanged.

We propose that by comparing the key distinguishing features of the various EHD flows as summarized in Table 2, with characteristics observed from experiments, one can easily identify the dominant mechanism that is responsible for driving the fluid flow, at least for certain imposed conditions.

Acknowledgement

Funding for this project through the Australian Research Council Discovery Project Grants DP0666660 and DP0773221 is acknowledged.

References

[1] T.M. Squires, S.R. Quake, Microfluidics: Fluid physics at the nanoliter scale, Reviews of Modern Physics 77 (2005) 977–1026.
[2] Y. Feng, J. Seyed-Yagoobi, Understanding of electrohydrodynamic conduction phenomenon, Physics of Fluids 16 (2004) 2432–2441.
[3] K. Takemura, S. Yokota, K. Edamura, A micro artificial muscle actuator using electro-conjugate fluids, in: International Conference on Robotics and Automation, 2005, pp. 532–537.
[4] Y. Otsubo, K. Edamura, Dielectric fluid motors, Applied Physics Letters 71 (1997) 318–320.
[5] S. Yokota, Y. Kondoh, A. Sadamoto, Y. Otsubo, K. Edamura, A micro motor using electro-conjugate fluids (ECF) (proposition of stator electrode-type (SE-type) micro ECF motors), JSME International Journal Series C 44 (2001) 756–762.
[6] J.R. Melcher (ed.), Continuum Electromechanics, 1981.
[7] E.B. Baker, H.A. Bolts, Thermionic emissions into dielectric liquids, Physical Review 51 (1937) 275–284.
[8] O.M. Stuetzer, Ion-drag pressure generation, Journal of Applied Physics 30 (1959) 984–994.
[9] P. Foroughi, V. Benetis, V. Ohadi, Design, testing and optimization of a micropump for cryogenic spot cooling applications, in: 21st Annual IEEE Semiconductor Thermal Measurement and Management Symposium, 2005, pp. 335–340.
[10] J. Darabi, H. Wand, Development of an electrohydrodynamic injection micropump and its potential application in pumping fluids in cryogenic cooling systems, Journal of Microelectromechanical Systems 14 (2005) 747–755.
[11] J. Seyed-Yagoobi, Jeong. S., Theoretical/numerical study of electrohydrodynamic pumping through conduction phenomenon, IEEE Transactions on Industry Applications 39 (2003) 355–361.
[12] R. Raghavan, J. Qin, L.Y. Yeo, J.R. Friend, K. Takemura, S. Yokota, K. Edamura, Electrohydrodynamic actuation of low conductivity dielectric fluids, in: Proceedings of the ASME Sixth International Conference on Nanochannels, Microchannels and Minichannels, 2008, p. 62239.
[13] O.M. Stuetzer, Ion drag pumps, Journal of Applied Physics 31 (1960) 136–146.
[14] S.A.S. Al Dini, Electrohydrodynamic induction and conduction pumping of dielectric liquid film: theoretical and numerical studies, Ph.D. Thesis, Texas A & M University, 2005.

[15] L. Onsager, Deviations from Ohm's law in weak electrolytes, Journal of Chemical Physics 2 (1934) 599–615.
[16] K. Reiss, Versuche zum Stromleitungsmechanismus in Flüssigkeiten niedriger Dielektrizitätskonstante, Annalen der Physik 420 (4) (1937) 325–342.
[17] J. Seyed-Yagoobi, P. Atten, J.E. Bryan, Y. Feng, B. Malraison, Electrohydrodynamically induced dielectric liquid flow through pure conduction in point/plane geometry—experimental study, in: 13th International Conference on Dielectric Liquids, 1999, pp. 548–551.
[18] H.J. Plumley, Conduction of electricity by dielectric liquids at high field strengths, Physical Review 59 (1941) 200–207.
[19] H.-C. Chang, Electrokinetics: a viable microfluidic platform for miniature diagnostic kits, Canadian Journal of Chemical Engineering 84 (2006) 146–160.
[20] J.R. Melcher, Travelling-wave induced electroconvection, Physics of Fluids 9 (1966) 1548–1555.
[21] J.M. Crowley, P. Chang, D. Riley, J.C. Chato, EHD induction pumping in annuli, IEEE Transactions on Electrical Insulation 20 (1985) 413–418.
[22] H.-C. Chang, L.Y. Yeo, Electrokinetically-driven microfluidics and nanofluidics, Cambridge University Press, Cambridge, in press, ISBN-13: 9780521860253, http://cambridge.org/us/catalogue/catalogue.asp?isbn=0521860253.
[23] L.Y. Yeo, H.-C. Chang, Electrowetting on parallel line electrodes, Physical Review E 73 (2006) 011605.
[24] G. Cho, D. Kim, S. Kang, Electric field solutions between an emitter tip and a plane extractor in LMIS, Journal of Physics D: Applied Physics 23 (1990) 85–89.
[25] H.A. Pohl, Dielectrophoresis, Cambridge University Press, Cambridge, 1978.
[26] D.R. Lide (Ed.), CRC Handbook of Chemistry and Physics, CRC Press, 2003.
[27] D.V. Rosato, N.R. Schott, M.G. Rosato, Plastics Engineering, Manufacturing & Data Handbook, 2nd Edition, Springer, 2001, 1751.
[28] S.W. Bigelow, Handbook of Plastics, second ed., Van Nostrand, 1949.

Biographies

Rohan Raghavan is a Master's student in the Department of Mechanical and Aerospace Engineering at Monash University. His research interests include the application of electrokinetics and surface acoustic waves to the development of microactuators and microfluidic devices.

Jiaxing Qin is currently completing his BE (Biomedical) degree at the University of Melbourne. He has been a research student at MNRL, Monash University under the supervision of Associate Professor James Friend and Dr. Leslie Yeo. His current research focuses on the effects of surface acoustic waves on protein crystallisation.

Leslie Yeo is currently an Australian Research Fellow and Senior Lecturer in the Department of Mechanical & Aerospace Engineering and Co-Director of the Micro/Nanophysics Research Laboratory at Monash University, Australia. He received his PhD from Imperial College London in 2002, for which he was awarded the Dudley Newitt prize for a computational/theoretical thesis of outstanding merit. Prior to joining Monash University, he was a Mathematical Modeller at Det Norske Veritas UK and a postdoctoral research associate in the Department of Chemical & Biomolecular Engineering at the University of Notre Dame, USA. Dr. Yeo was the recipient of the 2007 Young Tall Poppy Science Award from the Australian Institute for Policy & Science 'in recognition of the achievements of outstanding young researchers in the sciences including physical, biomedical, applied sciences, engineering and technology', and a finalist in the 2008 Eureka Prize People's Choice Award. Dr. Yeo is the author of over 70 research publications and over 10 patent applications, and is currently the Co-Editor of the American Institute of Physics journal Biomicrofluidics.

James Friend received the B.S. degree in aerospace engineering, and the M.S. and Ph.D. degrees in mechanical engineering from the University of Missouri-Rolla in 1992, 1994, and 1998, respectively. He received two awards – the AIAA Jefferson Student Goblet and ASME Presentation Award – for his presentation on ultrasonic motor analysis at the AIAA/ASME/AHS/ASC 26th Annual Structural Dynamics Conference in 1996, an award for the encouragement of young scientists at the Symposium for Ultrasonic Electronics and Engineering in 2003 for a presentation on acoustic waveguides, an award in 2004 for a presentation on the Scream actuator at the Spring Meeting of the Acoustical Society of Japan, excellence in teaching and early career researcher awards from the Monash Faculty of Engineering in 2007 and 2008, respectively, and a Future Leader award from the Davos Future Summit in Sydney in 2008. James Friend joined Monash University in late 2004, and founded and co-directs the $6.5 million MicroNanophysics Research Laboratory with clean room and biolab, a current staff of three academics, three post-doctorates and thirteen PhD students. He is an associate professor and deputy head of the Department of Mechanical and Aerospace Engineering at Monash University, with research interests in micro/nanodevices for biomedical applications, with over one hundred peer-reviewed publications, with five book chapters, fifty-two peer-reviewed journal papers, and thirteen patents and patent applications.

Kenjiro Takemura received his B.E. degree in mechanical engineering and M.S. degree in biomedical engineering from Keio University, Yokohama, Japan in 1998 and 2000, respectively. He also received his Ph.D. degree in integrated design engineering from Keio University in 2002. He was with the Precision & Intelligence Laboratory at Tokyo Institute of Technology from 2003 to 2008 as an Assistant Professor. Since 2008, he has been with the Department of Mechanical Engineering at Keio University, where he is currently an Assistant Professor. His research interest is on new actuators, robotics and mechatronics.

Shinichi Yokota received his Ph.D. degree in mechanical engineering from Tokyo Institute of Technology in 1982. He was with the Research Laboratory of Precision Machinery and Electronics at Tokyo Institute of Technology as a Research Associate from 1975 to 1986. Since 1986, he has been with the Precision and Intelligent Laboratory also at Tokyo Institute of Technology, where he is currently a Full Professor. His research interest is on micro actuators using functional fluids, fluid power mechatronics.

Kazuya Edamura received his M.S. degree in Chemical Engineering from Tokyo Institute of Technology in 1978. After his career as a chemist in the Research Lab. at Kyowa Hakko Kogyo Co., Ltd. and a Product Manager in Diagnostics Dept. Boehringer Mannheim Japan, he found the New Technology Management Co., Ltd. His main works are on ECF technology, MRF technology, ERF technology, etc.